Pressure-Impulse Diagram Method – A Fundamental Review

Accepted manuscript doi:
10.1680/jencm.17.00017

Submitted: 29 September 2017

Published online in 'accepted manuscript' format: 26 February 2019

Manuscript title: Pressure-Impulse Diagram Method – A Fundamental Review

Authors: Leon Chernin[1], Margi Vilnay[2], Igor Shufrin[3] and Demitrios Cotsovos[4]

Affiliations: [1]School of Science and Engineering, University of Dundee, Dundee, UK; [2]School of Science, Engineering and Technology, Abertay University, UK; [3]Department of Structural Engineering, Faculty of Engineering Sciences, Ben-Gurion University of the Negev, Israel and [4]School of Energy, Geoscience, Infrastructure and Society, Heriot Watt University, UK

Corresponding author: Leon Chernin, School of Science and Engineering, University of Dundee, Dundee, UK. Tel.: +44(0)1382 384922, Fax: +44(0)1382 384389.

E-mail: l.chernin@dundee.ac.uk

Accepted manuscript doi:
10.1680/jencm.17.00017

Abstract

Accidental and deliberate explosions stemming from catastrophic events in the petroleum industry, incidents during complex manufacturing processes, mishandling or failure of domestic gas appliances or installations, terrorist attacks and military engagements, are becoming increasingly relevant in structural design. Pressure-impulse (P-I) diagrams are widely used for the preliminarily assessment and design of structures subjected to such extreme loading conditions. A typical P-I diagram provides information concerning the level of damage sustained by a specific structural member when subjected to a blast load. This paper presents a state-of-the-art review describing the development of the P-I diagram method over the last 70 years, the main assumptions upon which its development is based and the framework through which such the method is applied in practice. The structural analysis methods used for the derivation of P-I curves are discussed and the existing approaches are categorised according to algorithms used. A review of the P-I curve formulae proposed to date is performed, where the formulae are classified according to the formulation methods.

Keywords: Pressure-impulse diagram; Blast load; Damage; Structural analysis; Classification

Accepted manuscript doi:
10.1680/jencm.17.00017

1. Introduction

Analysis of extensive air blast tests conducted during 1940's and 1950's at Aberdeen Proving Ground in Maryland, USA (Sperrazza, 1951) and damage caused to houses by bombs dropped on the UK during the Second World War (Jarrett) indicated that P-I diagrams were well suited to describe the damage caused by explosions. In early applications, the P-I diagrams derived from the analysis of blast damaged brick houses were applied for the assessment of small civil and industrial buildings (Jarrett). Further attempts to derive P-I diagrams for structures, humans and military targets using experimental, analytical and numerical methods were made in 1950's (Symonds, 1953; Hodge, 1956), 60's (Sperrazza, 1963; Johnson, 1967; Bowen *et al.*, 1968; Richmond *et al.*, 1968; White, 1968), 70's (Damon *et al.*, 1970; Youngdahl, 1970; White *et al.*, 1971; Baker, 1973; Westine and Baker, 1975; Westine and Cox, 1975; Abrahamson and Lindberg, 1976; BRL, 1976; Schumacher and Cummings, 1977; Baker *et al.*, 1978) and 80's (Baker *et al.*, 1983; Command, 1986; Zhu *et al.*, 1986). Nowadays, the P-I diagram method is used for the assessment of the loading regime, the ultimate load and the post-loading condition of structures subjected to blast loads (Hodge, 1956; Abrahamson and Lindberg, 1976; Baker *et al.*, 1978; Baker *et al.*, 1983; Departments of the Army, 1990; TNO, 1992; USDE, 1992; Mays and Smith, 1995; CCPS, 1996; ASCE, 1997; Q. Li and Meng, 2002a; Q. M. Li and Meng, 2002b; Ng and Krauthammer, 2004; Soh and Krauthammer, 2004; Nystrom, 2006; Blasko *et al.*, 2007; Campidelli and Viola, 2007; Fallah and Louca, 2007; G. W. Ma *et al.*, 2007; Krauthammer *et al.*, 2008; PDC, 2008; Yanchao Shi *et al.*, 2008; USACE, 2008; Cormie *et al.*, 2009; El-Dakhakhni *et al.*, 2009; Razaqpur *et al.*, 2009; CCPS, 2010; Dusenberry, 2010; X Huang *et al.*, 2010; G. Ma *et al.*, 2010; Yanchao Shi *et al.*, 2010; Mutalib and Hao, 2011; H. J. Shi *et al.*, 2012; Astarlioglu *et al.*, 2013; Ding *et al.*, 2013; Fallah *et al.*, 2013; Nassr *et al.*, 2013; Thiagarajan *et al.*, 2013; Xihong Zhang *et al.*, 2013), as well as for evaluation of the safe stand-off distance using additional 'range-charge weight' overlays (Abrahamson and Lindberg, 1976; Mays and Smith, 1995; Cormie *et al.*, 2009). This method relates the structural response of beams, plates, shells and other structural elements to an applied load with a specific peak pressure and impulse (Westine and Baker, 1975; Westine and Cox, 1975; BRL, 1976) and is recommended by various design codes (Command, 1986; Departments of the Army, 1990; TNO, 1992; USDE, 1992; CCPS, 1996; ASCE, 1997; PDC, 2008; USACE, 2008; Dusenberry, 2010). Each curve in the P-I diagram describes a certain degree of structural damage and can also be used for assessment of structural safety and survivability.(Bowen *et al.*, 1968; Richmond *et al.*, 1968; White, 1968; Damon *et al.*, 1970; White *et al.*, 1971).

This paper presents a fundamental review of the P-I diagram method used for the assessment of structures subjected to blast loads. Initially, a comprehensive discussion of the P-I diagram method is presented, followed by a review of the existing approaches adopted to date for derivation of P-I diagrams. These approaches are categorised according to the techniques and algorithms used. Finally, an extensive state-of-the-art review of existing P-I curve formulae is provided, where the formulae are classified according to their formulation methods.

2. P-I diagram method

The P-I diagram is a particular case of a more general *load-impulse* diagram (Abrahamson and Lindberg, 1976; Krauthammer, 2008; Krauthammer *et al.*, 2008). However, the popularity of the P-I diagram method led to the use of this term even when other types of loads were considered (Baker *et al.*, 1983; Mays and Smith, 1995; Thilakarathna *et al.*, 2010).

Accepted manuscript doi:
10.1680/jencm.17.00017

The P-I diagrams are usually built for single structural elements, e.g., beams, columns, walls, plates, etc., though the application of P-I diagrams to frames (Command, 1986) and even whole buildings (Ambrosini *et al.*, 2005) is also possible (though the latter approach lacks generality as it is case dependent). Essentially, the P-I diagram, also called an *iso-damage* curve, is built for a unique combination of loads acting on a specific structure and for a specific level of damage and type of failure. This method is found to be sensitive to various structural and numerical parameters including:

- geometrical dimensions (Wesevich and Oswald, 2005; Yanchao Shi *et al.*, 2008; Thilakarathna *et al.*, 2010; Colombo and Martinelli, 2012; W. Wang *et al.*, 2012b; Jun Li and Hao, 2013; Stolz *et al.*, 2014)
- ductility (Krauthammer *et al.*, 2008; Razaqpur *et al.*, 2009; El-Dakhakhni *et al.*, 2010; Stolz *et al.*, 2014)
- strain rate (Razaqpur *et al.*, 2009)
- damping ratio (Krauthammer *et al.*, 2008; G. Ma *et al.*, 2010)
- stiffness (Yu *et al.*, 2018)
- longitudinal and hoop reinforcement ratios (Symonds, 1953; Yanchao Shi *et al.*, 2008; Colombo and Martinelli, 2012; Jun Li and Hao, 2013)
- reinforcement configuration (Wesevich and Oswald, 2005; Thiagarajan *et al.*, 2013)
- material nonlinearity (X Huang *et al.*, 2010; Dragos and Wu, 2013; Dragos *et al.*, 2013; Dragos and Wu, 2014; Parlin *et al.*, 2014)
- concrete strength (Symonds, 1953; Yanchao Shi *et al.*, 2008; Colombo and Martinelli, 2012; Jun Li and Hao, 2013; Parlin *et al.*, 2014)
- reinforcement strength (Symonds, 1953; Yanchao Shi *et al.*, 2008)
- strength and thickness of fibre reinforced polymer retrofitting wraps and strips (Mutalib and Hao, 2011)
- axial force (Fallah and Louca, 2007; El-Dakhakhni *et al.*, 2009; Astarlioglu *et al.*, 2013; Chernin *et al.*, 2016; Yu *et al.*, 2018)
- bending and shear capacity (Gombeda *et al.*, 2017; Yu *et al.*, 2018)
- number of degrees of freedom (El-Dakhakhni *et al.*, 2010)
- load time history (Youngdahl, 1970; Abrahamson and Lindberg, 1976; Zhu *et al.*, 1986; Q. Li and Meng, 2002a; Q. M. Li and Meng, 2002b; Nystrom, 2006; Campidelli and Viola, 2007; Fallah and Louca, 2007; W. Wang *et al.*, 2012a; Dragos *et al.*, 2013; Fallah *et al.*, 2013; Parlin *et al.*, 2014; Chernin *et al.*, 2016).

This sensitivity can partially be considered by building additional curves reflecting the variation in a certain parameter, e.g. (Sperrazza, 1963; Campidelli and Viola, 2007; Krauthammer *et al.*, 2008; Yanchao Shi *et al.*, 2008; El-Dakhakhni *et al.*, 2009; El-Dakhakhni *et al.*, 2010; G. Ma *et al.*, 2010; Mutalib and Hao, 2011; Colombo and Martinelli, 2012; Astarlioglu *et al.*, 2013; Thiagarajan *et al.*, 2013). Other solutions included using P-I bands (El-Dakhakhni *et al.*, 2009), building three dimensional diagrams (Campidelli and Viola, 2007; Fallah and Louca, 2007; El-Dakhakhni *et al.*, 2009; Ding *et al.*, 2013; Nassr *et al.*, 2013; Parisi, 2015) and applying various normalisation techniques (Youngdahl, 1970; Q. Li and Meng, 2002a; Q. M. Li and Meng, 2002b; Campidelli and Viola, 2007; G. W. Ma *et al.*, 2007; X Huang *et al.*, 2010; G. Ma *et al.*, 2010; H. J. Shi *et al.*, 2012; Fallah *et al.*, 2013; Yu *et al.*, 2018). The latter method is discussed in Sections 3.3 and 4.1.

A typical shape of the P-I diagram as illustrated in Fig. 1 is close in shape to a rectangular hyperbola. Note that the abscissa of the diagram in Fig. 1 is normalised against the maximum impulse, while the ordinate against maximum quasi-static pressure. In the figure, G is the

Accepted manuscript doi:
10.1680/jencm.17.00017

limit state function representing the degree of structural damage which can be expressed as (Q. Li and Meng, 2002a; Q. M. Li and Meng, 2002b; Rhijnsburger *et al.*, 2002; Ng and Krauthammer, 2004; Soh and Krauthammer, 2004; Blasko *et al.*, 2007; G. W. Ma *et al.*, 2007; Fallah *et al.*, 2013)

$$G(I,P) = \lambda/\lambda_{max} \quad (1)$$

where λ is the failure criterion. The situation when $G \geq 1$ corresponds to the state of structural failure and $G < 1$ to limited damage. G can also represent the degree of structural survivability or safety if its formulation in Eq. (1) is changed to $G(I,P) = 1 - \lambda/\lambda_{max}$ (Hodge, 1956; Fallah and Louca, 2007). Different research studies used different definitions for λ, e.g. the principle deflection at midspan of a structural element (Abrahamson and Lindberg, 1976; Baker *et al.*, 1978; Baker *et al.*, 1983; Command, 1986; Conrath *et al.*, 1999; Q. Li and Meng, 2002a; Q. M. Li and Meng, 2002b; Wesevich and Oswald, 2005; Nystrom, 2006; Campidelli and Viola, 2007; Fallah and Louca, 2007; G. W. Ma *et al.*, 2007; Yanchao Shi *et al.*, 2008; El-Dakhakhni *et al.*, 2010; G. Ma *et al.*, 2010; H. J. Shi *et al.*, 2012; Astarlioglu *et al.*, 2013; Dragos and Wu, 2013; Dragos *et al.*, 2013; Jun Li and Hao, 2013; Nassr *et al.*, 2013; Thiagarajan *et al.*, 2013; Dragos and Wu, 2014; Parlin *et al.*, 2014; Stolz *et al.*, 2014; Hamra *et al.*, 2015; Chernin *et al.*, 2016; Syed *et al.*, 2016; Gombeda *et al.*, 2017; Xin Huang *et al.*, 2017) or at its supports (G. W. Ma *et al.*, 2007; G. Ma *et al.*, 2010; H. J. Shi *et al.*, 2012; W. Wang *et al.*, 2012b; Jun Li and Hao, 2013), the maximum sideway deflections (Command, 1986), the maximum rotations (Command, 1986; Moghimi and Driver, 2015; Liu *et al.*, 2018; Yu *et al.*, 2018), the residual axial load-carrying capacity (Yanchao Shi *et al.*, 2008; Mutalib and Hao, 2011; Ding *et al.*, 2013), the maximum strain (Hooper *et al.*, 2012; Xihong Zhang *et al.*, 2013), von-Mises yielding criterion (Baker *et al.*, 1978; Baker *et al.*, 1983) and Tresca yielding criterion (Zhu *et al.*, 1986).

A typical P-I curve can be divided into a vertical asymptote, a hyperbolic curve and a horizontal asymptote as shown in Fig. 1. These three parts represent the different loading regimes: (I) impulsive, (II) dynamic and (III) (quasi-)static (Baker *et al.*, 1983; Q. Li and Meng, 2002a; Campidelli and Viola, 2007; Yanchao Shi *et al.*, 2008; Cormie *et al.*, 2009; El-Dakhakhni *et al.*, 2009; El-Dakhakhni *et al.*, 2010; Yanchao Shi *et al.*, 2010; Mutalib and Hao, 2011; Dragos and Wu, 2014); and can also be called (I) impulse controlled, (II) pressure-impulse controlled and (III) pressure controlled regime (USACE, 2008) based on the orientation of the asymptotes.

The impulsive and (quasi-)static asymptotes are the distinctive features of the P-I curves. For a normalised P-I diagram, the position of the horizontal asymptote varies from 0.5 to 1.0 depending on the load rise time (Krauthammer, 2008; Chernin *et al.*, 2016). When the load increases slowly without generating inertia effects, the asymptote crosses the normalised pressure axis at 1.0 and is called static. When the load has zero rise time, i.e., step load, the inertia effects are generated and the asymptote crosses the normalised pressure axis at 0.5. This asymptote is called quasi-static. For a load with a relatively short rise time (time from load start to peak) the position of the horizontal asymptote is in between 0.5 and 1.0 depending on the degree of the inertia effects generated (Q. Li and Meng, 2002a; Q. M. Li and Meng, 2002b; Campidelli and Viola, 2007; Fallah and Louca, 2007; Krauthammer, 2008; Yanchao Shi *et al.*, 2008; El-Dakhakhni *et al.*, 2010; Yanchao Shi *et al.*, 2010; Mutalib and Hao, 2011; Dragos and Wu, 2013; Dragos *et al.*, 2013; Fallah *et al.*, 2013; Dragos and Wu, 2014; Chernin *et al.*, 2016). With increasing ductility, the quasi-static asymptote approaches the static asymptote due to the increasing amount of energy absorbed by plastic deformations (Krauthammer, 2008). Hereafter, the horizontal asymptote is referred to as static or quasi-

Accepted manuscript doi:
10.1680/jencm.17.00017

static depending on the shape of the pulse load used in diagram derivation. When the loading regime is unclear, the asymptote is referred to as (quasi-)static.

The P-I curve in the dynamic domain is also sensitive to the load rise time (Q. Li and Meng, 2002a; Q. M. Li and Meng, 2002b; Krauthammer, 2008; Krauthammer *et al.*, 2008; Chernin *et al.*, 2016). The load with the finite rise time results in a series of peaks and dips in the elbow of the curve (Krauthammer, 2008) since the limit state condition $G = 1$ is reached during different natural periods of structural vibration. The impulsive asymptote is not insensitive to the load rise time (Baker *et al.*, 1978; Baker *et al.*, 1983).

3. Derivation of P-I diagrams

The derivation of P-I diagrams consists of two stages. First, the structural analysis is used to assess the level of damage, thus creating a point on the P-I plane. Second, the next most suitable point on the P-I plane is searched for using an algorithm. The methods of structural analysis and search algorithms are discussed in this section.

3.1. Methods of structural analysis

There are three general methods of structural analysis that are commonly applied for the derivation of single points on the P-I plane. They include experimental, analytical and numerical modelling. The experimental method (Wesevich and Oswald, 2005; Hooper *et al.*, 2012; Parlin *et al.*, 2014; Stolz *et al.*, 2014) has limited application because of budget constraints and strict safety requirements of blast tests. Therefore, the number of tests is limited, while the test data is often significantly scattered and not sufficient for derivation of a whole P-I curve. The high scatter predominantly reflects the difficulty in correlating the measured response to the actual physical state of specimens. For instance, the measured maximum value of imposed load frequently corresponds to a specimen physical-state characterised by high material disintegration as well as low residual load-bearing capacity and stiffness (Cotsovos, 2010; Cotsovos and M.N., 2012). This stage of structural response has little practical significance as it depends heavily on post-failure mechanisms for transferring the applied loads to the specimen supports. Thus, the available test data cannot provide detailed insight into the mechanisms underlying RC structural response. These drawbacks led to the development of supporting analytical and numerical methods for extending the limited sets of test data to be suitable for derivation of P-I diagrams.

It is important to note that the equivalence between the SDOF models and the structural members they represent is based upon energy approximations that rely on an assumed deflected shape (e.g. the first eigenvector or the deflected shape under equivalent static loading). The latter methodology relies on several simplifications concerning both the material behaviour and structural response. These include the use of simple uniaxial material laws, empirical amplification factors (attributed to the strain-rate sensitivity characterising material behaviour), assumptions concerning the deformed shape of the structural elements and elastic or elasto-plastic laws for describing structural behaviour. However, such simplifications prevent the methodology from accounting for the true behaviour of relevant materials or the true mechanics governing structural response, especially in the case of members constructed from brittle materials such as concrete and masonry.

The simplest analytical method is based on a single-degree-of-freedom (SDOF) model (Biggs, 1964; Abrahamson and Lindberg, 1976; Baker *et al.*, 1978; Baker *et al.*, 1983; Mays and Smith, 1995; Q. Li and Meng, 2002a; Q. M. Li and Meng, 2002b; Nystrom, 2006; G. W. Ma *et al.*, 2007; Yanchao Shi *et al.*, 2008; USACE, 2008; Cormie *et al.*, 2009; El-Dakhakhni *et al.*, 2010; H. J. Shi *et al.*, 2012; Dragos and Wu, 2013; Dragos *et al.*, 2013; Fallah *et al.*, 2013; Thiagarajan *et al.*, 2013; Dragos and Wu, 2014; Parlin *et al.*, 2014; Hamra *et al.*, 2015;

Accepted manuscript doi:
10.1680/jencm.17.00017

Gombeda *et al.*, 2017; Liu *et al.*, 2018) that simulates the dominant structural response. This model disregards the effects of the local modes of failure, which can lead to an inaccurate prediction of the post-loading structural condition, especially when the loading is impulsive (G. W. Ma *et al.*, 2007; Yanchao Shi *et al.*, 2008; El-Dakhakhni *et al.*, 2010; H. J. Shi *et al.*, 2012; Thiagarajan *et al.*, 2013). More complex structural behaviour was achieved using a few separate SDOF systems and selecting the most conservative response (Abrahamson and Lindberg, 1976). Another approach consisted in developing an analytical model with two coupled SDOF systems. This enabled to consider the effect of two interacting dominant modes of failure, e.g. the shear and flexural modes of a RC beam subjected to a localised impact load (H. J. Shi *et al.*, 2012) and of a RC slab under uniformly distributed blast loads (Ng and Krauthammer, 2004). Further increase in complexity of the analytical method, as an attempt in increasing their accuracy, was achieved by considering transverse velocity fields generated during failure of a rigid-plastic beam (G. W. Ma *et al.*, 2007; Xin Huang *et al.*, 2017; Yu *et al.*, 2018). This enabled to consider multiple shear, flexural and combined modes of failure (see Section 4.1) for further discussion). Chernin at el. (Chernin *et al.*, 2016) used an alternative analytical approach for modelling a beam-column, which was based on the continuous formulation and the Euler-Bernoulli beam theory. This approach enabled studying the behaviour of columns subjected to a combination of axial and blast loads and allowed to incorporate geometrical imperfections into the model.

The most popular numerical approach for derivation of P-I diagrams is the finite element (FE) method (Yanchao Shi *et al.*, 2008; Hao *et al.*, 2010; Yanchao Shi *et al.*, 2010; Mutalib and Hao, 2011; Astarlioglu *et al.*, 2013; Ding *et al.*, 2013; Nassr *et al.*, 2013; Thiagarajan *et al.*, 2013; Xihong Zhang *et al.*, 2013; Syed *et al.*, 2016; Yu *et al.*, 2018) due to its capability to catch both global and local failure modes. However, FE analysis usually employs dense 3D finite element meshes, combined with complex constitutive material laws implemented using iterative solution strategies and as a result the computational resources required for solving such problems is high. Consequently, the use of FE method is generally limited to the analysis of relatively simple structural forms. Moreover, the accuracy of the predictions obtained from FE analysis highly depends on the numerical description of material behaviour. The material models are derived either directly from the regression analyses of experimental data or based on continuum mechanics theories (i.e. nonlinear elasticity, plasticity, visco-plasticity and damage mechanics). The latter approach requires calibration of several model parameters, which is usually done using relevant experimental data. However, when considering brittle materials (i.e. concrete or masonry), the latter parameters are usually associated with post-failure behaviour (i.e. strain softening, tension stiffening, shear-retention ability) while often incorporating empirical amplification factors to account for the effect of strain-rate sensitivity on material behaviour (Michael *et al.*, 2008). The values of these parameters are often established through calibration based on the use of experimental information at the structural – rather than at the material – level. The use of such parameters tends to attribute ductile characteristics not compatible with the brittle nature of the materials considered and not justified by the relevant published test data (Michael *et al.*, 2008). This, in turn, can detrimentally affect the objectivity of the numerical predictions obtained, since such parameters often require recalibration depending on the type of problem investigated.

To avoid the complications and uncertainties associated with the FE analysis, to simplify the analysis and design procedures and to reduce the computational resources required for solving such problems, several techniques have been suggested up till now. In (Campidelli and Viola, 2007; Krauthammer, 2008; Cormie *et al.*, 2009; W. Wang *et al.*, 2012a; Ding *et al.*, 2013), the detailed FE model was substituted by an equivalent SDOF model with a

Accepted manuscript doi:
10.1680/jencm.17.00017

similar displacement-resistance function for modelling individual structural elements with distributed mass and loading. Li and Hao (J. Li and Hao, 2011) developed a two-step technique where the loading phase was analysed with an elastic-plastic SDOF system, while the post-loading phase using a detailed FE model. El-Dakhakhni et al. (El-Dakhakhni *et al.*, 2010) used the finite differences numerical method for the analysis of a multiple degree of freedom system obtained through the discretisation of a structure into segments.

3.2. Search Algorithms

Derivation of P-I curves requires generation of multiple points on the P-I plane by multiple analyses. To make the process of curve derivation more efficient, various search algorithms can be applied. These search algorithms can be divided into basic and advanced. The basic (or unidirectional) algorithms rely on generating a sufficient number of threshold points followed by curve fitting using single or multi-parametric regression techniques and can be computationally expensive. The derivation of P-I curves with the basic algorithms can be performed using either a pressure-controlled, an impulse-controlled or a mixed unidirectional search, as shown in Fig. 2.

The pressure-controlled search is based on the gradual increase of the duration of the blast load t_0 (and hence its impulse) in each simulation, while maintaining the peak pressure P_0 constant (see Fig. 3a). The duration t_0 is increased till the limit state condition $G \leq 1$ (see Eq. (1)) is satisfied. This search results in a horizontal series of points on the P-I plane for each P_0 (see Fig. 2). The impulse-controlled search is based on the gradual increase of P_0 in each simulation till $G \geq 1$. In this case, t_0 is gradually decreased to keep the impulse I constant (see Fig. 3b). This search algorithm results in a vertical series of points on the P-I plane generated for each I (see Fig. 2). In the mixed search, both P_0 and I (and so t_0) gradually increase in accordance with a certain linear proportionality rule $P_0 = \alpha I$ (see Fig. 3c), where α is a proportionality coefficient. This search algorithm results in a series of points along an inclined line emerging from the origin of the P-I coordinates (see Fig. 2). The inclination angle of the line is governed by α.

Fig. 2 shows an illustrative example of the derivation of a P-I curve for 70% structural damage (G = 0.7). As can be seen, the pressure-controlled approach is a horizontal searching algorithm, the impulse-controlled approach is a vertical searching algorithm, whereas the mixed approach is a polar search algorithm. Thus, the pressure-controlled search is especially suitable for derivation of the impulsive asymptote, the impulse-controlled search for the (quasi-)static asymptote, while the mixed search for the part of the P-I curve in the dynamic regime. In practice, the pressure-controlled search is the most popular approach used in many studies (e.g., (Yanchao Shi *et al.*, 2008; Yanchao Shi *et al.*, 2010; Mutalib and Hao, 2011; Ding *et al.*, 2013; Thiagarajan *et al.*, 2013; Xihong Zhang *et al.*, 2013; Fangrui Zhang *et al.*, 2017)) probably due to the convenience of changing only one parameter, i.e., t_0. A few research works (e.g., (Yanchao Shi *et al.*, 2008; Moghimi and Driver, 2015)) applied a combination of pressure-controlled and impulse-controlled searching algorithms.

The advanced search algorithms can be divided into two types of searching procedures: the point-to-point progress (Rhijnsburger *et al.*, 2002) and single point search (Ng and Krauthammer, 2004; Soh and Krauthammer, 2004; Blasko *et al.*, 2007). They are based on direct tracing of points on the P-I curve using numerical techniques (e.g. the bisection method) and differ in numerical stability and computational cost.

Accepted manuscript doi:
10.1680/jencm.17.00017

4. Classification of P-I diagrams

The P-I diagrams can be classified according to their formulation into three groups: single analytical expression, piecewise analytical expression and piecewise mixed formulation. The first formulation describes the whole P-I curve by a single formula, while the second usually requires two formulae valid in different regions. In the mixed formulation, the P-I diagram is described in the impulsive and (quasi-)static loading regimes by analytical expressions and derived numerically in the dynamic regime.

4.1. Single analytical expression

One of the first P-I diagram formulae was suggested by Sperrazza (Sperrazza, 1951) based on the analysis of the results of blast tests

$$(P_0 - P_{cr})(I - I_{cr}) = C \tag{2}$$

where P_0 is the peak pressure, I is the total impulse delivered by the blast, i.e., the area under the pulse load time history $P(t)$; P_{cr} and I_{cr} are the values of the (quasi-)static and impulsive asymptotes, respectively, and C is the constant determined from the fitting to experimental results. The total impulse I was defined in an integral form as

$$I = \int_{t_s}^{t_f} P(t)dt \tag{3}$$

where t_s and t_f are the times of the start and finish of the part of the $P(t)$ curve with $P(t) > P_{cr}$.

The expression (2) was found to be sensitive to the shape of the $P(t)$ curve (Hodge, 1956; Westine and Cox, 1975; TNO, 1992; ASCE, 1997), which prompted the development of methods where similar loading conditions yield similar P-I diagrams. Based on the analysis of rigid-plastic structures (beams, circular plates, circular and cylindrical shells) under transient distributed and localised loads, Youngdahl (Youngdahl, 1970) suggested to eliminate the shape dependency by introducing an additional parameter derived from the pulse load time history, namely, the characteristic time $\bar{t}$ defined as

$$\bar{t} = \frac{1}{I}\int_{t_s}^{t_f}(t - t_s)P(t)dt \tag{4}$$

Note that $\bar{t}$ represents the location of the centroid of the critical pulse loading area corresponding to the time of the onset of the critical displacement, t_s. To determine t_s and t_f when the $P(t)$ curve had complex shape, Youngdahl introduced an iterative procedure based on the equality

$$P_y(t_f - t_s) = \int_{t_s}^{t_f} P(t)dt \tag{5}$$

where P_y is the static yield load. This procedure was based on the condition of zero initial velocity. As the expression (2) was already widely used in the military engineering community, Youngdahl adjusted the extended description of the blast-induced structural damage to

$$(\bar{P} - P_{cr})(I - I_{cr}) = C \tag{6}$$

where $\bar{P}$ is the normalised pressure defined as

$$\bar{P} = I/(2\bar{t}) \tag{7}$$

Accepted manuscript doi:
10.1680/jencm.17.00017

It is important to note that Eqs. (3), (4) and (7) transform an arbitrary load time history to an equivalent rectangular shape with the constant pressure $\bar{P}$ and duration $\bar{t}$. Youngdahl validated his method using several idealised load time histories including rectangular, triangular, exponential and sinusoidal.

Schumacher and Cummings (Schumacher and Cummings, 1977) simplified the expression (6) by setting $P_{cr} = I_{cr} = 0$ when P_{cr} and I_{cr} were not known. This lead to the expression

$$\bar{P}I = DN \tag{8}$$

where DN is the damage number depending only on the pulse pressure.

Abrahamson and Lindberg (Abrahamson and Lindberg, 1976) modified the expression (2) into the form of a rectangular hyperbola

$$(P_0/P_{cr} - 1)(I/I_{cr} - 1) = 1 \tag{9}$$

Eq. (9) represents a normalised P-I diagram Eq. (2) plotted in the $P_0/P_{cr} - I/I_{cr}$ plane. Eq. (9) approximated well only the response of simple structures such as beams and plates which can be accurately represented by equivalent linear elastic and rigid plastic SDOF systems. The P-I diagram showed sensitivity to the $P(t)$ shape in the dynamic part with the deviation reaching 20-40%.

Li and Meng (Q. Li and Meng, 2002a) reduced the sensitivity of the P-I diagram to idealised shapes of the load time history through normalisation of governing parameters. The non-dimensional diagram had the form

$$p = n_1/(i-1)^{n_2} + 0.5 \tag{10}$$

where p and i are the non-dimensional equivalent pressure and impulse, defined as

$$p = P_0/(u_{cr}K) \tag{11}$$

$$i = I/\left(u_{cr}\sqrt{MK}\right) = p\int_0^{\tau_0} P(\tau)/P_0 d\tau \tag{12}$$

$$\tau_0 = t_0/\sqrt{M/K} \tag{13}$$

where t_0 is the loading duration and u_{cr} the critical structural deflection. n_1 and n_2 were derived as second order polynomial functions of I and $\bar{t}$ from Eqs. (3) and (4), respectively, using the least-square fitting of Eq. (10) to the response of an undamped elastic SDOF system with mass M and stiffness K. The proposed method works efficiently only for elastic structures subjected to loads with idealised time histories. It is limited by the single-parameter definition of the load shape and the sensitivity of the normalised P-I curves to the relationship between the load function and the structural response (Campidelli and Viola, 2007; Krauthammer *et al.*, 2008; Dragos *et al.*, 2013). The influence of the load-response relationship becomes especially pronounced in the dynamic and the quasi-static regions of the P-I curve.

Accepted manuscript doi:
10.1680/jencm.17.00017

Later, Li and Meng (Q. M. Li and Meng, 2002b) extended their approach (Q. Li and Meng, 2002a) to elastic-plastic SDOF systems whose response was governed by the dimensionless parameters $\bar{p} = P_0/R_{cr}$ and $\upsilon = R_{cr}/(u_{cr}K)$, where R_{cr} is the critical resistance. For the rigid-perfectly plastic system response, the normalised P-I diagram was formulated as

$$1/\bar{p} + (u_m/u_{cr})(2/i^2) = 1/\upsilon \tag{14}$$

with

$$\bar{p} = \frac{i}{(2\bar{\tau})} \tag{15}$$

$$\bar{\tau} = \frac{p}{i}\int_0^{\tau_0} \tau P(\tau)/\, P_0 d\tau \tag{16}$$

where p, i and τ_0 are defined in Eqs. (11-13), and u_m is the maximum deflection achieved by the structure. The P-I diagram in Eq. (14) is sensitive to the shape of the load time history in the dynamic loading regime. The ratio R_{cr}/K in the expression for υ represents the elastic yield deflection, which is constant for a given material. As a result, the P-I diagram is influenced by u_{cr} (through υ) even when $u_m/u_{cr} = 1$. The authors eliminated this influence by transforming the limit state function $G(i,p)$ into $G(i/h_2(\upsilon), p/h_1(\upsilon))$, where $h_1(\upsilon)$ and $h_2(\upsilon)$ were the quadratic functions of υ derived for the idealised load time histories using the method of least squares.

The next step in the development of the analytical P-I diagrams was coupled with the use of advanced structural analysis techniques. Ma et al. (G. W. Ma *et al.*, 2007) derived separate P-I diagrams for the shear and bending failure of simply supported and fully clamped rigid-plastic beams using the mode approximation method. The analytical formulation of the beam was based on the transverse velocity fields generated by five distinct failure modes. The failure modes depended on the end support conditions, the beam bending strength M_{cr}, its half span L, the applied pressure p_0 and the dimensionless shear-to-bending strength ratio $\upsilon = LV_{cr}/2M_{cr}$. The normalised P-I diagrams had the forms

$$\alpha/i_e^2 + 1/p_e = f_1(\upsilon) \qquad \text{for shear failure} \tag{17}$$

$$k\beta/i_e^2 + 1/p_e = f_2(\upsilon) \qquad \text{for bending failure} \tag{18}$$

where

$$i_e = I/\sqrt{2mV_{cr}} = I\sqrt{L/4m\upsilon M_{cr}} \tag{19}$$

$$p_e = p_0 L/V_{cr} = p_0 L^2/(2\upsilon M_{cr}) \tag{20}$$

and $\alpha = u_s/L$ and $\beta = u_{ms}/L$ are the normalised beam deflections at supports u_s and mid-span u_{ms}; $f_1(\upsilon)$ and $f_2(\upsilon)$ depend on the end support conditions, the failure mode and its transverse velocity profile, V_{cr} the shear strength of the beam and m the mass per unit length. In Eq. (18), $k = 2/3$ when the beam fails by developing bending hinges at the supports, otherwise $k = 1$. The P-I diagrams (17) and (18) agreed well with the elastic-plastic SDOF model describing only the simple bending failure especially when the large peak pressure and impulse were applied and severe damage developed. Additionally, the uncoupling of the failure modes and the use of idealised pulse shapes limit the applicability of this method.

Accepted manuscript doi:
10.1680/jencm.17.00017

Shi et al. (H. J. Shi *et al.*, 2012) incorporated the combined shear-flexural response patterns into the beam model in (G. W. Ma *et al.*, 2007), thus increasing the number of failure modes to 12. The diagrams (17) and (18) were transformed into more general forms

$$[\varphi_1(p_e)\cdot\alpha/i_e^2]^{\lambda_1}+k_1/p_e=f_1(\upsilon,p_e) \quad \text{for shear failure} \quad (21)$$

$$[\varphi_2(p_e)\cdot\beta/i_e^2]^{\lambda_2}+k_2/p_e=f_2(\upsilon,p_e) \quad \text{for bending failure} \quad (22)$$

where $p_c=2M_{cr}/L^2$ is the collapse pressure; (f_1, φ_1, λ_1) and (f_2, φ_2, λ_2) are two sets of parameters depending on the end support conditions, the type of failure and its transverse velocity profile. The comparison with an equivalent SDOF model describing the beam failure in pure shear and bending showed that the SDOF model was inaccurate for the combined shear-bending failure modes corresponding to $1\le\upsilon\le 1.5$. Later, this approach was extended by Huang et al. (Xin Huang *et al.*, 2017) to derivation of P-I diagrams for RC slabs under blast loads using the mode approximation method.

Fallah et al. (Fallah *et al.*, 2013) adopted the P-I diagram in Eq. (10) to describe the response of continuous simply supported beams to pulse loads with idealised time histories. The diagram (10) was modified into a more general form

$$p=n_1/(i-C)^{n_2}+C \quad (23)$$

where

$$p=P_0l^4/\left(u_{crp}EI\right) \quad (24)$$

$$i=I/\left(u_{crp}\sqrt{EIm/(\kappa l^2)}\right) \quad (25)$$

u_{crp} is the critical plastic deflection, l is the beam length and EI is the beam bending stiffness. C equals 1 for elastic and 10 for elastic-perfectly plastic beams. The order of polynomials n_1 and n_2 is increased to the third. $\kappa=K_\theta l/EI$ defines the order of development of the plastic hinges at supports and mid-span, where K_θ is the stiffness of elastic-plastic rotational springs at supports representing the influence of neighbouring spans. The diagram (23) still had the limitation of the diagram (10).

Shi et al. (Yanchao Shi *et al.*, 2008) performed an extensive numerical study on RC columns under a triangular pulse pressure load. The authors suggested, based on the least-square curve fitting of the FE results, a P-I diagram expression

$$(P_0-P_{cr})(I-I_{cr})=C(P_{cr}/2+I_{cr}/2)^D \quad (26)$$

where C and D are the constants obtained for three degrees of damage: 20%, 50% and 80%. Here 20% was considered as the boundary between low and medium damage, 50% between medium and high damage, while 80% between high damage and structural collapse. Each part of the P-I curve represented different type of column failure, i.e. in the impulsive loading regime the column failed in shear, in the quasi-static loading regime in bending, while in the dynamic loading regime in the combined shear-flexural mode. C and D showed low sensitivity to the applied load, and $C=12$ and $D=1.5$ were suggested. P_{cr} and I_{cr} were derived form an extensive parametric study as highly nonlinear multiparametric functions for 20%, 50% and 80% damage.

Accepted manuscript doi:
10.1680/jencm.17.00017

The P-I diagram (26) was used in several research studies for assessment of damage in the reliability analysis of RC columns subjected to blast loads (Hao *et al.*, 2010), for RC columns retrofitted with fibre reinforced polymer strips and wraps (Mutalib and Hao, 2011), for steel columns with a box-type section exposed to blast followed by fire (Ding *et al.*, 2013), for the investigation of blast resistance of rectangular laminated glass windows (Xihong Zhang *et al.*, 2013), for ultra-high performance concrete filled double-skin steel tube columns under blast loading (Fangrui Zhang *et al.*, 2017). In each study, the values of C and D, and the expressions of P_{cr} and I_{cr} were derived for the structure considered.

Thiagarajan et al. (Thiagarajan *et al.*, 2013) developed P-I diagrams for RC columns subjected to blast loads with idealised time histories using advanced detailed FE analysis and a SDOF model. The authors focused on the effect of stirrups on column response. To achieve better fit to the analysis results, the authors introduced a logarithmic form of the P-I diagram and substituted I with t_0,

$$\log(p_r) = A + B \times \Delta + C \times Col + D \times \log(t_0) + E \times \log(t_0^2) + F \times \log(t_0^3) \quad (27)$$

where p_r is the reflected pressure; A, B, C, D and E are regression coefficients depending on the configuration of stirrups and Δ $(= 0.1 \div 5.25\%)$ is the damage level of the column. Unfortunately, the authors did not provide in their paper the values and meanings of the parameters F and Col.

Wang and Xiong (Yonghui Wang and Xiong, 2015) suggested another logarithmic form of the P-I diagram based on linear polynomial fitting of the SDOF system describing the response of a water storage tank to a triangular pulse pressure load

$$\ln(p-1) + 0.59\ln(i-1) + 1.07 = 0 \quad (28)$$

More accurate fitting in the dynamic part of the curve was achieved using the quadratic polynomial

$$\ln(p-1) + 0.026\ln^2(i-1) + 0.59\ln(i-1) + 0.97 = 0 \quad (29)$$

where

$$p = 4P_0/\left(k_{ep}\chi_m^3\right) \quad (30)$$

$$i = \left(2I^2/k_{ep}m_e\right)^{0.75}\chi_m^3 \quad (31)$$

Here $m_e = \kappa_{LM}\rho w l^2$, $k_{ep} = 21.104Et$ and $\chi_m = u_m/l$ are, respectively, the equivalent non-dimensional mass, plastic stiffness and maximum displacement of the SDOF system; κ_{LM} is the load-mass factor, w and l are the thickness and side length of the square tank wall; ρ and E are the density and Young's modulus of the tank material; and u_m is the maximum midspan displacement of the wall. Note that Eq. (28) can be transformed into the form similar to Eq. (2)

$$(p-1)(i-1)^{0.59} = 0.34 \quad (32)$$

Accepted manuscript doi:
10.1680/jencm.17.00017

4.2. Piecewise analytical formulation

The first type of the piecewise analytical formulation describes a P-I diagram using two analytical expressions, which represent a fundamental change in structural response due to the change of the loading regime. Zhu et al. (Zhu *et al.*, 1986) analysed three different types of simply supported rigid perfectly plastic structures subjected to uniform pressure loads with idealised time histories. The authors used Youngdahl's approach (Youngdahl, 1970) in development of the normalised P-I diagrams

$$\frac{6}{5}\left(\frac{I}{I_{cr}}\right)^2\left(1-\frac{P_y}{\bar{P}}\right)=1 \qquad \text{when } P_y/\bar{P}\le 2 \tag{33}$$

$$\left(\frac{I}{I_{cr}}\right)^2\left(1-\frac{4P_y}{5\bar{P}}\right)=1 \qquad \text{when } P_y/\bar{P}\ge 2 \tag{34}$$

where I and $\bar{P}$ are respectively given in Eqs. (3) and (7), respectively. The static yield load P_y was estimated using the Tresca yield criterion. To eliminate the uncertainty concerning the integration limits t_s and t_f in Eq. (4), $\bar{t}$ was calculated by integrating over the whole time interval, i.e., [0, ∞),

$$\bar{t}=\frac{1}{I}\int_0^\infty tP(t)dt \tag{35}$$

The formulae (33) and (34) drawn for different structures produced less than 5% scatter. However, the sensitivity to the load time history was more significant especially in the dynamic and impulsive parts of the P-I curves.

Vaziri et al. (Vaziri *et al.*, 1987) developed normalised P-I diagrams describing the response of axially restrained, rigid perfectly plastic beams to pressure pulse loads. The authors proposed a few sets of analytical expressions for the P-I diagrams depending on the supporting conditions, location of plastic hinges, level of damage and mode of response. In the case of the small damage and the simply supported end conditions, the P-I diagram was formulated as

$$\beta=\frac{p^2}{\sqrt{3(p-1)}}F^2\left(1/\sqrt{2},\phi\right) \qquad \text{for } 1<p\le 3 \tag{36}$$

$$\frac{1}{30}(\beta/p)^3+(\beta/p)\left[\frac{1}{2}-\frac{2}{3}p\right]+u_f/h+\frac{4}{3}\left(u_f/h\right)^3=0 \qquad \text{for } p\ge 3 \tag{37}$$

where $p=P_0/P_{cr}$ and $\beta=I^2/(mhP_0)$ are the non-dimensional pressure and impulse, respectively; $F\left(1/\sqrt{2},\phi\right)$ is the incomplete elliptic integral of the first kind with the modulus $1/\sqrt{2}$ and the amplitude $\phi=\phi\left(p,u_f/h\right)$, p_{cr} is the nondimensional critical static pressure, m is the mass per unit length of the beam, u_f is the final deflection, h was the beam depth, and I is defined in Eq. (3). Note that Eq. (36) corresponds to the bending mode, while Eq. (37) to the string mode. The P-I diagram expressions became more complex with increasing complexity of structural response and were non-conservative for low intensity loads with durations close to the fundamental period of vibrations of the elastic beam.

The second type of the piecewise analytical formulation uses three different analytical expressions to describe the P-I diagram in the three loading regimes. In this method, formulas are derived for the impulsive and (quasi-)static asymptotes, while curve fitting is used in the dynamic regime. Krauthammer et al. (Krauthammer, 2008; Krauthammer *et al.*, 2008) applied the normalisation technique developed in (Q. Li and Meng, 2002a) for derivation of

Accepted manuscript doi:
10.1680/jencm.17.00017

the expressions for the impulsive and static asymptotes based on the free and forced vibration responses of an undamped elastic SDOF system subjected to a rectangular load pulse

$$p\sin(0.5i/p) = 0.5 \qquad 1 \le i \le 0.5\pi \qquad \text{impulsive asymptote} \qquad (38)$$

$$p = 0.5 \qquad i > 0.5\pi \qquad \text{static asymptote} \qquad (39)$$

where p and i are defined in Eqs. (11) and (12). The transition between the asymptotes takes place at the point ($i = 0.5\pi,\ p = 0.5$). A more complex set of expressions was obtained when the pulse load had a triangular shape, i.e.

$$(2i/p^2)^2 = 2 + (2i/p)^2 - (4i/p)\sin(2i/p) - 2\cos(2i/p) \quad 1 \le i \le 1.166 \qquad (40)$$

$$(2i/p) = \tan[(2i/p)(1 - 0.5/p)] \qquad i > 1.166 \qquad (41)$$

Another approach is based on the principle of conservation of mechanical energy (Baker *et al.*, 1978; Baker *et al.*, 1983; Fallah and Louca, 2007; Krauthammer, 2008; Krauthammer *et al.*, 2008; Colombo and Martinelli, 2012), where the impulsive and (quasi-)static loading regimes are described by two distinct energy formulations. This approach uses an undamped elastic SDOF system representing a considered structure. The impulsive asymptote is derived from the assumption that the kinetic energy T is balanced in the conservative SDOF system by the potential energy represented in terms of the total strain energy E, i.e., $T = E$. The quasi-static asymptote is derived from the condition that the maximum work W done by the applied load P_0 to move the system to its final displacement u_f equals the total strain energy gained, i.e., $W = E$. For the undamped elastic SDOF system with mass M and stiffness K, the parameters T, E and W have the forms

$$T = I^2/2M \qquad E = Ku_f^2/2 \qquad W = P_0 u_f \qquad (42)$$

For an elastic-perfectly plastic SDOF system, the expression for E is (Colombo and Martinelli, 2012)

$$E = Ku_{el}\left(u_f - u_{el}/2\right) \qquad (43)$$

where u_f is divided into its elastic u_{el} and plastic $\left(u_f - u_{el}\right)$ parts. Using Eqs. (42) and that $T = E$ and $W = E$, the dimensionless impulsive and quasi-static asymptotes are $i = 1$ and $p = 0.5$, respectively. The expressions of the impulsive and (quasi-)static asymptotes derived for several other idealised SDOF systems can be found elsewhere (Soh and Krauthammer, 2004; Krauthammer, 2008; Dragos and Wu, 2013).

The P-I curve in the dynamic domain is approximated by several analytic functions. Hyperbolic functions are used for approximation of systems subjected to triangular and exponential load pulses. Baker et al. (Baker *et al.*, 1978; Baker *et al.*, 1983) used the hyperbolic tangent squared relationship

$$E = W\tanh^2\sqrt{T/W} \qquad (44)$$

Accepted manuscript doi:
10.1680/jencm.17.00017

For the small values of the argument, $\tanh\sqrt{T/W} \approx \sqrt{T/W}$ and Eq. (44) approaches the impulsive asymptote, while for the higher values of the argument, $\tanh\sqrt{T/W} \approx 1$ and Eq. (44) reduces to the quasi-static asymptote.

Oswald and Skerkut (Oswald and Sherkut, 1994) approximated the dynamic part of the normalised P-I curve derived for a SDOF system under a triangular pulse load with the formula similar to Eq. (26), i.e.

$$(p - p_{cr})(i - i_{cr}) = 0.4(0.5p_{cr} + 0.5i_{cr})^{1.5} \quad (45)$$

where p_{cr} and i_{cr} are the values of the normalised static and impulsive asymptotes, respectively. Krauthammer (Krauthammer, 2008) further generalised this expression to

$$(p - p_{cr})(i - A_i) = C(p_{cr} + i_{cr})^D \quad (46)$$

where

$$p_{cr} = 0.5, i_{cr} = 1.0, C = 0.01, D = 1.0 \quad \text{for rectangular pulse} \quad (47)$$

$$p_{cr} = 0.5, i_{cr} = 1.0, C = 0.08, D = 0.3 \quad \text{for triangular pulse} \quad (48)$$

4.3. Piecewise mixed formulation

In the piecewise mixed formulation, the impulsive and (quasi-)static asymptotes are given as analytical expressions, while the P-I curve in the dynamic domain is derived numerically using curve fitting of FE analysis results or a SDOF system and a search algorithm (see Section 3.2). Falllah and Louca (Fallah and Louca, 2007) combined the approaches from (Q. Li and Meng, 2002a) and (Baker *et al.*, 1978; Baker *et al.*, 1983) in deriving the normalised P-I diagrams for a three-pitch corrugated stainless steel blast wall based on the dimensional analysis of a complex elastic-plastic SDOF system under pulse loads with idealised time histories. The static and impulsive asymptotes were defined as

$$p = \eta(1 - \varphi\psi^2) + 0.5\varphi(\psi^2 - \varphi\eta^2 + \eta^2\psi^2) \quad \text{static asymptote} \quad (49)$$

$$i = \sqrt{2\eta(1 - \varphi\psi^2) + \varphi(\psi^2 - \varphi\eta^2 + \eta^2\psi^2)} \quad \text{impulsive asymptote} \quad (50)$$

where p and i are defined in Eqs. (20) and (21), $\eta = u_y/u_{cr}$ is the inverse ductility, $\psi^2 = K_{h(s)}/K$ the hardening/softening index, u_y the deflection at the yielding and $K_{h(s)}$ the hardening/softening stiffness. φ = 1 corresponded to the hardening behaviour, while φ = -1 to the softening. The P-I curve in the dynamic domain was obtained by fitting the bilinear response of the SDOF system to the nonlinear response of the FE model. At least one point in the dynamic domain was required for completing the fitting procedure, which was based on numerical integration of the SDOF and FE resistance-displacement functions.

Colomboa and Martinelli (Colombo and Martinelli, 2012) applied the search algorithm proposed in (Blasko *et al.*, 2007) for derivation of the P-I diagrams describing the response of RC and fibre-reinforced concrete circular plates under blast loads. The static and impulsive asymptotes were formulated using the energy-based approach (see Section 5.2) as

$$P = \frac{R_{cr}(u_f - u_{el}/2)}{L^*_{el}u_{el} + L^*_{pl}(u_f - u_{el})} \quad \text{static asymptote} \quad (51)$$

$$I = \left[2mR_{cr}(u_f - u_{el}/2)/(\pi r^2)\right]^{1/2} \quad \text{impulsive asymptote} \quad (52)$$

Accepted manuscript doi:
10.1680/jencm.17.00017

where $R_{cr} = Ku_{el}$ is the critical (yielding) resistance force, u_f and u_{el} the final and elastic deflections, m the mass per unit area and r the plate radius. L^*_{el} and L^*_{pl} are the elastic and plastic load multiplier coefficients obtained using load generalisation with shaper functions.

Li and Hao (Jun Li and Hao, 2013) applied an elastic-plastic SDOF system for derivation of the impulsive asymptote used for evaluation of damage in simply supported RC beams at the end of the blast loading phase. The information from the asymptote was then used in the FE analysis of the beams in the post-loading phase to correct the concrete strength and its Young's modulus in the shear damage zones. The asymptote was formulated as

$$P = a \times I + b \tag{53}$$

where the coefficients a and b were found through fitting the results of a parametric study using multi-parametric regression analysis for damage levels between 10%-50%.

Conclusions

This paper presents a fundamental review of the pressure-impulse (P-I) diagrams where special attention is given to challenges facing engineers in the development of the method. The detailed description of the P-I diagrams provides an insight into their strengths and weaknesses. The P-I diagram method has been used for characterisation of damage in various structures such as beams, plates, columns, walls. P-I diagrams are sensitive by different geometrical, structural, material and loading parameters. The techniques for reduction of this sensitivity are summarised. The methodologies adopted for deriving P-I diagrams include experimental, analytical (single degree of freedom model) and numerical (finite element method) approaches. The weaknesses of these approaches associated with the adopted simplifications (concerning material and structural behaviour) as well as the uncertainties associated with the ability of the available numerical and experimental data (used for calibration purposes) to accurately describe structural response under blast loading are discussed. The search algorithms used for analytically defining the profile of the P-I curves are classified into pressure-controlled, impulse controlled and mixed. Finally, the P-I diagram equations are categorised into those described by a single or piecewise analytical expression and those using a piecewise mixed formulation; the former being much easier to apply compared to the latter two due to smaller number of parameters required for their calibration.

Accepted manuscript doi:
10.1680/jencm.17.00017

Notations

G the limit state function
λ the failure criterion
I the total impulse
I_{cr} the impulsive asymptotes
i non-dimensional equivalent impulse
t the time
$\bar{t}$ the characteristic time
P_0 the peak pressure
P_y the static yield load
$\bar{P}$ the normalised pressure
P_{cr} the (quasi-)static asymptote
p the non-dimensional equivalent pressure
p_0 the non-dimensional applied pressure
p_c the collapse pressure
p_{cr} the nondimensional critical static pressure
t_0 the loading duration
M the mass of a single degree of freedom system
m the mass per unit length
m_e the equivalent non-dimensional mass of a single degree of freedom (SDOF) system
K the stiffness of a single degree of freedom system
K_θ the stiffness of elastic-plastic rotational springs at supports
k_{ep} the equivalent non-dimensional plastic stiffness of a SDOF system
R_{cr} the critical resistance
M_{cr} the beam bending strength
V_{cr} the shear strength of the beam
u_m the maximum deflection achieved by the structure
u_{cr} the critical structural deflection
u_f the final deflection
u_s the beam deflections at support
u_{ms} the beam deflections at midspan
u_{crp} the critical plastic deflection
u_{el} the elastic displacement
u_y the yielding deflection
χ_m the equivalent non-dimensional maximum displacement of a SDOF system
α the normalised beam deflection at support
β the normalised beam deflection at support
w the thickness of the square tank wall
l the side length of the square tank wall
ρ the density
E the Young's modulus
η the inverse ductility
ψ the hardening/softening index

υ the dimensionless shear-to-bending strength ratio
DN the damage number
L the beam half span
h the beam depth
$h_{1(2)}$ the quadratic function of υ
$n_{1(2)}$ the second order polynomial function of I and $\bar{t}$
T the kinetic energy
E the strain energy
W the maximum work
κ_{LM} the load-mass factor
L_{el}^{*} the elastic load multiplier coefficient
L_{pl}^{*} the plastic load multiplier coefficient
A, B, C, D, E, F the constants

References

Abrahamson, G. R. and Lindberg, H. E. (1976) 'Peak load-impulse characterization of critical pulse loads in structural dynamics', *Nuclear Engineering and Design*, 37, pp. 35-46.

Ambrosini, D., Luccioni, B., Jacinto, A. and Danesi, R. (2005) 'Location and mass of explosive from structural damage', *Engineering Structures*, 27(2), pp. 167-176.

ASCE (1997) 'Design of Blast Resistant Buildings in Petrochemical Facilities' Design, T. C. o. B. R. New York, NY: American Society of Civil Engineers.

Astarlioglu, S., Krauthammer, T., Morency, D. and Tran, T. P. (2013) 'Behavior of reinforced concrete columns under combined effects of axial and blast-induced transverse loads', *Engineering Structures*, 55, pp. 26-34.

Baker, W. E. (1973) *Explosion in air*. Austin, Texas: University of Texas Press.

Baker, W. E., Cox, P. A., Westine, P. S., Kulesz, J. J. and Strehlow, R. A. (1978) *A Short Course on Explosion Hazards Evaluation*. San Antonio, Texas: Southwest Research Institute.

Baker, W. E., Cox, P. A., Westine, P. S., Kulesz, J. J. and Strehlow, R. A. (1983) *Explosion hazards and evaluation*. London: Elsevier.

Biggs, J. M. (1964) *Introduction to Structural Dynamics*. New York: McGraw-Hill Book Company.

Blasko, J., Krauthammer, T. and Astarlioglu, S. (2007) *Pressure-impulse diagrams for structural elements subjected to dynamic loads* (PTC-TR-002-2007). University Park, Pennsylvania, PA.

Bowen, I. G., Fletcher, E. R. and Richmond, D. R. (1968) *Estimate of Man's Tolerance to the Direct Effects of Air Blast* (DASA 2113) (AD 693105).

BRL (1976) 'Energy Approaches to Structural Vulnerability with Application of the New Bell Stress - Strain Laws' Greenspon, J. E. USA Ballistic Research Laboratories.

Campidelli, M. and Viola, E. (2007) 'An analytical–numerical method to analyze single degree of freedom models under airblast loading', *Journal of Sound and Vibration*, 302(1-2), pp. 260-286.

CCPS (1996) 'Guidelines for Evaluating Process Plant Buildings for External Explosions and Fires'. New York, NY: Center for Chemical Process Safety (CCPS), American Institute of Chemical Engineers.

CCPS (2010) *Guidelines for Vapor Cloud Explosion, Pressure Vessel Burst, BLEVE and Flash Fire Hazards*. 2 edn. Edited by Center for Chemical Process Safety (CCPS), A. I. o. C. E. New Jersey: Wiley & Sons.

Chernin, L., Vilnay, M. and Shufrin, I. (2016) 'Blast dynamics of beam-columns via analytical approach', *International Journal of Mechanical Sciences*, 106, pp. 331-345.

Colombo, M. and Martinelli, P. (2012) 'Pressure--impulse diagrams for RC and FRC circular plates under blast loads', *European Journal of Environmental and Civil Engineering*, 16(7), pp. 837-862.

Command, N. F. E. DESIGN MANUAL 2.08 (1986) 'Blast Resistant Structures'.

Conrath, E. J., Krauthammer, T., Marchand, K. A. and Mlakar, P. F. (1999) *Structural design for physical security: state of the practice*. Reston, VA: Structural Engineering Institute of American Society of Civil Engineers.

Cormie, D., Mays, G. and Smith, P. (2009) 'Blast Effects on Buildings - (2nd Edition)'. ICE Publishing.

Cotsovos, D. M. (2010) 'A simplified approach for assessing the load-carrying capacity of reinforced concrete beams under concentrated load applied at high rates', *International Journal of Impact Engineering*, 37(8), pp. 907-917.

Cotsovos, D. M. and M.N., P. (2012) 'Modelling of RC beams under impact loading', *Proceedings of the Institution of Civil Engineers - Structures and Buildings*, 165(2), pp. 77-94.

Damon, E. G., Yelverton, J. T., Luft, U. C. and Jones, R. K. (1970) *Recovery of the Respiratory System Following Blast Injury* (DASA 2580).

Departments of the Army, t. N. a. t. A. F. US Army Manual UFC 3-340-01 (1990) 'Design and Analysis of Hardened Structures to Conventional Weapons Effects'.

Ding, Y., Wang, M., Li, Z.-X. and Hao, H. (2013) 'Damage evaluation of the steel tubular column subjected to explosion and post-explosion fire condition', *Engineering Structures*, 55, pp. 44-55.

Dragos, J. and Wu, C. (2013) 'A new general approach to derive normalised pressure impulse curves', *International Journal of Impact Engineering*, 62, pp. 1-12.

Dragos, J. and Wu, C. (2014) 'Application of Normalized Pressure Impulse Diagrams for Vented and Unvented Confined Blasts', *Journal of Engineering Mechanics*, 140(3), pp. 593-603.

Dragos, J., Wu, C. and Vugts, K. (2013) 'Pressure-Impulse Diagrams for an Elastic-Plastic Member under Confined Blasts', *International Journal of Protective Structures*, 4(2), pp. 143-162.

Dusenberry, D. O. (2010) *Handbook for Blast Resistant Design of Buildings*. New Jersey: John Wiley & Sons.

El-Dakhakhni, W., Mekky, W. and Changiz-Rezaei, S. (2009) 'Vulnerability Screening and Capacity Assessment of Reinforced Concrete Columns Subjected to Blast', *Journal of Performance of Constructed Facilities*, 23(5), pp. 353-365.

El-Dakhakhni, W., Mekky, W. and Rezaei, S. (2010) 'Validity of SDOF Models for Analyzing Two-Way Reinforced Concrete Panels under Blast Loading', *Journal of Performance of Constructed Facilities*, 24(4), pp. 311-325.

Fallah, A. S. and Louca, L. A. (2007) 'Pressure–impulse diagrams for elastic-plastic-hardening and softening single-degree-of-freedom models subjected to blast loading', *International Journal of Impact Engineering*, 34(4), pp. 823-842.

Fallah, A. S., Nwankwo, E. and Louca, L. A. (2013) 'Pressure-Impulse Diagrams for Blast Loaded Continuous Beams Based on Dimensional Analysis', *Journal of Applied Mechanics*, 80(5), p. 051011.

Gombeda, M. J., Naito, C. J., Quiel, S. E. and Fallon, C. T. (2017) 'Blast-Induced Damage Mapping Framework for Use in Threat-Dependent Progressive Collapse Assessment of Building Frames', *Journal of Performance of Constructed Facilities*, 31(2).

Hamra, L., Demonceau, J. F. and Denoel, V. (2015) 'Pressure-impulse diagram of a beam developing non-linear membrane action under blast loading', *International Journal of Impact Engineering*, 86, pp. 188-205.

Hao, H., Stewart, M. G., Li, Z.-X. and Shi, Y. (2010) 'RC Column Failure Probabilities to Balst Loads', *International Journal of Protective Structures*, 1(4), pp. 571-591.

Hodge, P. (1956) 'The influence of blast characteristics on the final deformation of circular cylindrical shells', *Journal of Applied Mechanics, ASME*, 23, pp. 617-624.

Hooper, P. A., Sukhram, R. A. M., Blackman, B. R. K. and Dear, J. P. (2012) 'On the blast resistance of laminated glass', *International Journal of Solids and Structures*, 49(6), pp. 899-918.

Huang, X., Bao, H., Hao, Y. and Hao, H. (2017) 'Damage Assessment of Two-Way RC Slab Subjected to Blast Load Using Mode Approximation Approach', *International Journal of Structural Stability and Dynamics*, 17(01), p. 1750013.

Huang, X., Ma, G. W. and Li, J. C. (2010) 'Damage Assessment of Reinfoced Concrete Structural Elements Subjected to Blast Load', *International Journal of Protective Structures*, 1(1), pp. 103-124.

Jarrett, D. E. (1968) 'Derivation of the british explosives safety distances', *Annals of the New York Academy of Sciences*, 152(1), pp. 18-35.

Johnson, O. T. (1967) *A blast-damage relationship* (Report No. 1389). Maryland.

Krauthammer, T. (2008) *Modern Protective Structures*. Boca Raton: CRC Press.

Krauthammer, T., Astarlioglu, S., Blasko, J., Soh, T. B. and Ng, P. H. (2008) 'Pressure–impulse diagrams for the behavior assessment of structural components', *International Journal of Impact Engineering*, 35(8), pp. 771-783.

Li, J. and Hao, H. (2011) 'A Two-step Numerical Method for Efficient Analysis of Structural Response to Blast Load', *International Journal of Protective Structures*, 2(1), pp. 103-126.

Li, J. and Hao, H. (2013) 'Influence of brittle shear damage on accuracy of the two-step method in prediction of structural response to blast loads', *International Journal of Impact Engineering*, 54, pp. 217-231.

Li, Q. and Meng, H. (2002a) 'Pressure-Impulse Diagram for Blast Loads Based on Dimensional Analysis and Single-Degree-of-Freedom Model', *Journal of Engineering Mechanics*, 128(1), pp. 87-92.

Li, Q. M. and Meng, H. (2002b) 'Pulse loading shape effects on pressure–impulse diagram of an elastic–plastic, single-degree-of-freedom structural model', *International Journal of Mechanical Sciences*, 44, pp. 1985-1998.

Liu, L., Zong, Z. H., Tang, B. and Li, M. H. (2018) 'Damage Assessment of an RC Pier under Noncontact Blast Loading Based on P-I Curves', *Shock and Vibration*.

Ma, G., Huang, X. and Li, J. (2010) 'Simplified Damage Assessment Method for Buried Structures against External Blast Load', *Journal of Structural Engineering*, 136(5), pp. 603-612.

Ma, G. W., Shi, H. J. and Shu, D. W. (2007) 'P–I diagram method for combined failure modes of rigid-plastic beams', *International Journal of Impact Engineering*, 34(6), pp. 1081-1094.

Mays, G. and Smith, P. D. (1995) *Blast Effects on Buildings: Design of Buildings to Optimize Resistance to Blast Loading*. T. Telford.

Michael, K., Milija, P. and Demetrios, C. (2008) 'Characteristic features of concrete behaviour: implications for the development of an engineering finite-element tool', *Computers and Concrete*, 5(3), pp. 243-260.

Moghimi, H. and Driver, R. G. (2015) 'Performance assessment of steel plate shear walls under accidental blast loads', *Journal of Constructional Steel Research*, 106, pp. 44-56.

Mutalib, A. A. and Hao, H. (2011) 'Development of P-I diagrams for FRP strengthened RC columns', *International Journal of Impact Engineering*, 38(5), pp. 290-304.

Nassr, A. A., Razaqpur, A. G., Tait, M. J., Campidelli, M. and Foo, S. (2013) 'Strength and stability of steel beam columns under blast load', *International Journal of Impact Engineering*, 55, pp. 34-48.

Ng, P. H. and Krauthammer, T. (2004) *Pressure–impulse diagrams for reinforced concrete slabs* (PTC-TR-007-2004). University Park, Pennsylvania, PA.

Nystrom, U. (2006) *Design with regard to explosions*. MSc thesis. Chalmers University of Technology.

Oswald, C. J. and Sherkut, D. (1994) *FACEDAP theory manual*. Omaha, Nebraska.

Parisi, F. (2015) 'Blast fragility and performance-based pressure–impulse diagrams of European reinforced concrete columns', *Engineering Structures*, 103, pp. 285-297.

Parlin, N. J., Davids, W. G., Nagy, E. and Cummins, T. (2014) 'Dynamic response of lightweight wood-based flexible wall panels to blast and impulse loading', *Construction and Building Materials*, 50, pp. 237-245.

PDC PDC TR-08-07 (2008) 'Component Explosive Damage Assessment Workbook (CEDAW)'. Omaha, NE: US Army Corps of Engineers, Protective Design Center (PDC).

Razaqpur, G., Mekky, W. and Foo, S. (2009) 'Fundamental concepts in blast resistance evaluation of structuresThis article is one of a selection of papers published in the Special Issue on Blast Engineering', *Canadian Journal of Civil Engineering*, 36(8), pp. 1292-1304.

Rhijnsburger, M. P. M., van Deursen, J. R. and van Doormaal, J. C. A. M. (2002) 'Development of a toolbox suitable for dynamic response analysis of simplified structures', *30th DoD Explosives Safety Seminar*. Atlanta, GA.

Richmond, D. R., Damon, E. G., Fletcher, E. R., Bowen, I. G. and White, C. S. (1968) 'The Relationship Between Selected Blast Wave parameters and the Response of Mammals Exposed to Air Blast', *Annals of the New York Academy of Sciences*, 152, pp. 103-121.

Schumacher, R. N. and Cummings, B. E. (1977) *A MODIFIED PRESSURE-IMPULSE BLAST MODEL* (2724). Aberdeen, Maryland, USA.

Shi, H. J., Salim, H. and Ma, G. (2012) 'Using P-I Diagram Method to Assess the Failure Modes of Rigid-Plastic Beams Subjected to Triangular Impulsive Loads', *International Journal of Protective Structures*, 3(3), pp. 333-353.

Shi, Y., Hao, H. and Li, Z.-X. (2008) 'Numerical derivation of pressure–impulse diagrams for prediction of RC column damage to blast loads', *International Journal of Impact Engineering*, 35(11), pp. 1213-1227.

Shi, Y., Li, Z.-X. and Hao, H. (2010) 'A new method for progressive collapse analysis of RC frames under blast loading', *Engineering Structures*, 32(6), pp. 1691-1703.

Soh, T. B. and Krauthammer, T. (2004) *Pressure–impulse diagrams for reinforced concrete slabs* (PTC-TR-007-2004). University Park, Pennsylvania, PA.

Sperrazza, J. (1951) *Dependence of external blast damage to the A-25 Aircraft on peak pressure and impulse* (575). Maryland, USA.

Sperrazza, J. (1963) 'Modelling of Air Blast', *In Use of models and scaling in shock and vibration*. Philadelphia, Pennsylvania. Winter annual meeting of the ASME.

Stolz, A., Fischer, K., Roller, C. and Hauser, S. (2014) 'Dynamic bearing capacity of ductile concrete plates under blast loading', *International Journal of Impact Engineering*, 69, pp. 25-38.

Syed, Z. I., Mohamed, O. A. and Rahman, S. A. (2016) 'Non-linear Finite Element Analysis of Offshore Stainless Steel Blast Wall under High Impulsive Pressure Loads', *Icsdec 2016 - Integrating Data Science, Construction and Sustainability*, 145, pp. 1275-1282.

Symonds, P. (1953) 'Dynamic load characteristics in plastic bending of beams', *Journal of Applied Mechanics, ASME*, 20, pp. 475-481.

Thiagarajan, G., Rahimzadeh, R. and Kundu, A. (2013) 'Study of Pressure-Impulse Diagrams for Reinforced Concrete Columns using Finite Element Analysis', *International Journal of Protective Structures*, 4(4), pp. 485-504.

Thilakarathna, H. M. I., Thambiratnam, D. P., Dhanasekar, M. and Perera, N. (2010) 'Numerical simulation of axially loaded concrete columns under transverse impact and vulnerability assessment', *International Journal of Impact Engineering*, 37(11), pp. 1100-1112.

TNO (1992) 'Method for the Determination of Possible Damage to People and Objects Resulting from Releases of Hazardous Materials' Labour, D.-G. o. Voorburg: Committee for the Prevention of Disasters Due to Dangerous Substances.

USACE US Army Manual UFC 3-340-02 (2008) 'Structures to Resist the Effects of Accidental Explosions' US Army Corps of Engineering, N. F. E. C., Air Force Civil Engineer Support Agency.

USDE DOE/TIC- 11268 (1992) 'A Manual for the Prediction of Blast and Fragment Loadings on Structures'. US Department of Energy, Amarillo, Texas.

Vaziri, R., Olson, M. D. and Anderson, D. L. (1987) 'Dynamic response of axially constrained plastic beams to blast loads', *International Journal of Solids and Structures*, 23(1), pp. 153-174.

Wang, W., Zhang, D. and Lu, F. (2012a) 'The influence of load pulse shape on pressure-impulse diagrams of one-way RC slabs', *Structural Engineering and Mechanics*, 42(3), pp. 363-381.

Wang, W., Zhang, D., Lu, F., Wang, S. C. and Tang, F. (2012b) 'The effect of span length to height ratio of reinforced concrete slabs on pressure-impulse diagram with multiple failure modes under blast loading', *EPJ Web of Conferences*, 26, p. 04015.

Wang, Y. and Xiong, M.-X. (2015) 'Analysis of axially restrained water storage tank under blast loading', *International Journal of Impact Engineering*, 86, pp. 167-178.

Wesevich, J. W. and Oswald, C. J. (2005) *Proceeding of Structures Congress, ASCE*.

Westine, P. S. and Baker, W. E. (1975) *Energy Solutions for Predicting Deformations in Blast-Loaded Structures*.

Westine, P. S. and Cox, P. A. (1975) *Additional Energy Solutions for Predicting Structural Deformations*.

White, C. S. (1968) 'The Scope of Blast and Shock Biology and Problem Areas in Relating Physical and Biological Parameters', *Annals of the New York Academy of Sciences*, 152, pp. 89-102.

White, C. S., Jones, R. K., Damon, E. G., Fletcher, E. R. and Richmond, D. R. (1971) *The Biodynamics of Air Blast* (DNA 2738T).

Youngdahl, C. (1970) 'Correlation parameters for eliminating the effect of pulse shape on dynamic plastic deformation', *Journal of Applied Mechanics, ASME*, 37(3), pp. 744-752.

Yu, R. Q., Zhang, D. D., Chen, L. and Yan, H. C. (2018) 'Non-dimensional pressure-impulse diagrams for blast-loaded reinforced concrete beam columns referred to different failure modes', *Advances in Structural Engineering*, 21(14), pp. 2114-2129.

Zhang, F., Wu, C., Zhao, X.-L. and Li, Z.-X. (2017) 'Numerical derivation of pressure-impulse diagrams for square UHPCFDST columns', *Thin-Walled Structures*, 115, pp. 188-195.

Zhang, X., Hao, H. and Ma, G. (2013) 'Parametric study of laminated glass window response to blast loads', *Engineering Structures*, 56, pp. 1707-1717.

Zhu, G., Huang, Y. G., Yu, T. X. and Wang, R. (1986) 'Estimation of the plastic structural response under impact', *International Journal of Impact Engineering*, 4(4), pp. 271-282.

List of Figures

Accepted manuscript doi:
10.1680/jencm.17.00017

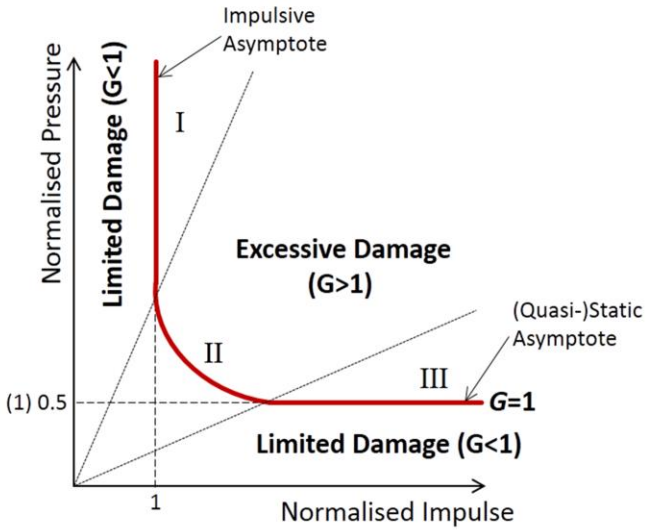

figure 01

Accepted manuscript doi:
10.1680/jencm.17.00017

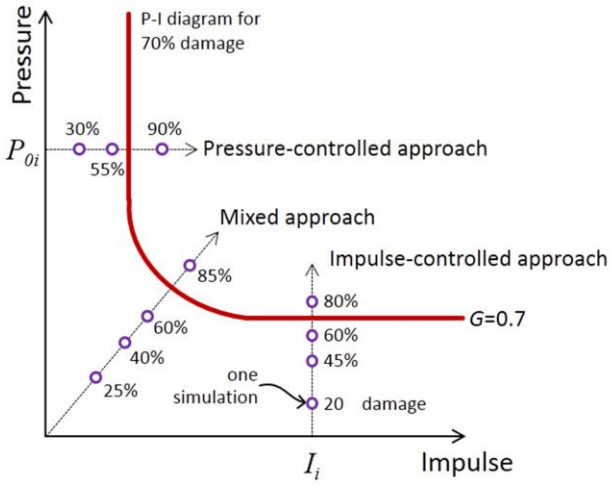

figure 02

Accepted manuscript doi:
10.1680/jencm.17.00017

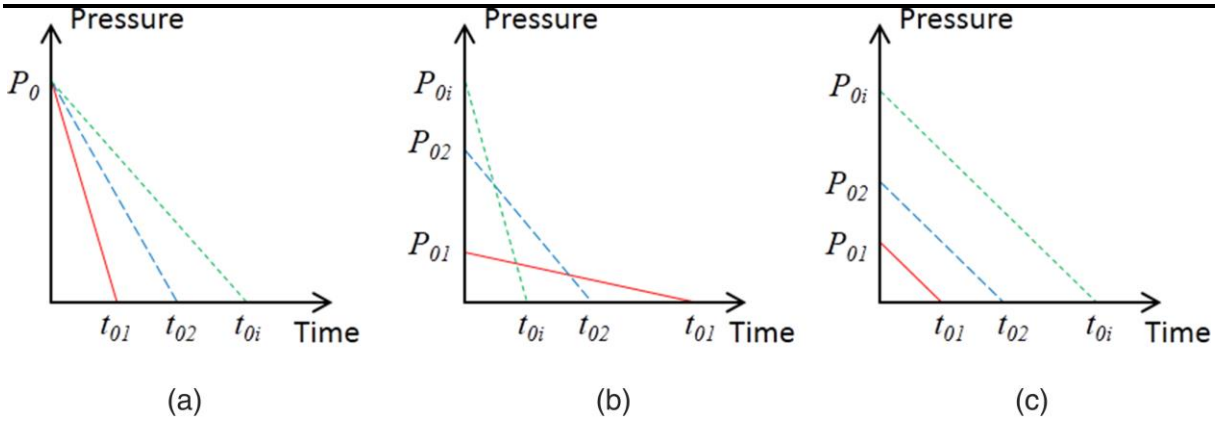

figure 03